Soft Matter

PAPER

View Article Online
View Journal | View Issue

Cite this: *Soft Matter*, 2025, **21**, 6058

Diverse nanostructures and antimicrobial activity of lipopeptides bearing lysine-rich tripeptide sequences†

Ian W. Hamley, *[a] Valeria Castelletto, [a] Callum Rowding,[a] Callum Wilkinson,[a] Lucas R. de Mello,[a] Bruno Mendes,[b] Glyn Barrett[b] and Jani Seitsonen[c]

The self-assembly and conformation in aqueous solution and bioactivity of three lipopeptides bearing lysine-rich tripeptide sequences are compared for C_{16}-KFK, C_{16}-KWK, and C_{16}-KYK, where C_{16} denotes an N-terminal hexadecyl (palmitoyl) chain. The central aromatic residue has a significant effect on the self-assembled nanostructures, since C_{16}-KFK forms nanotubes, whereas the other two lipopeptides form nanotapes. The nanotubes and nanotapes are built from lipopeptide bilayers, as confirmed by small-angle X-ray scattering. Circular dichroism (CD) spectroscopy and thioflavin T dye fluorescence show the presence of β-sheet structures, and the latter technique was used to determine critical aggregation concentrations (CACs). Fibre X-ray diffraction for C_{16}-KFK shows a well-defined helical diffraction pattern arising from the helically wrapped bilayers in the nanotube walls. The lipopeptides act as surfactants, as confirmed by surface tension measurements (also used to determine CAC values). All three lipopeptides show minimal cytotoxicity to human fibroblasts but also, unexpectedly, low activity against Gram-negative and Gram-positive bacteria, in contrast to previously studied analogues (with switch of two residues) C_{16}-WKK and C_{16}-YKK that show significant antimicrobial action with low minimum inhibitory concentration (MIC) values [A. Adak *et al.*, *ACS Appl. Bio Mater.*, 2024, **7**, 5553–5565]. Also in contrast to these molecules (which show a transition from micelles to fibrils upon increasing the pH), C_{16}-KFK, C_{16}-KWK, and C_{16}-KYK form extended β-sheet structures over the whole pH range examined (pH 2–8). These observations point to the remarkable sensitivity to the tripeptide pattern of lipopeptide self-assembly and antibacterial activity. Whereas the C_{16}-XKK (X = W or Y) lipopeptides form cylindrical fibrils, the C_{16}-KXK analogues form bilayer nanotapes. The former show significant toxicity to bacteria in contrast to the latter, which we propose is due to the effect of the lipopeptide assembly curvature on induced bacterial membrane deformation.

Received 28th April 2025,
Accepted 24th June 2025

DOI: 10.1039/d5sm00432b

rsc.li/soft-matter-journal

Introduction

Lipopeptide (LPP) molecules comprise a lipid hydrophobic chain attached to a peptide sequence leading to diverse properties resulting from a bio-derived or bio-inspired peptide sequence.[1] They have demonstrated selective anticancer activity,[2] collagen stimulation by fibroblasts,[3] selective antimicrobial activity,[4–12] and many other properties key to biomedicine and tissue engineering.[10,13–17]

LPPs self-assemble in solution above a critical aggregation concentration. Different lipid chain types, peptide sequences or solution conditions, can result in distinct self-assembly motifs,[1,13–15,18–22] which include nanofibrils, nanosheets and nanotubes. Our group and others have previously reported the self-assembly of several LPPs into nanofibrils, with a β-sheet secondary structure,[12,14,23–26] or micelles with generally unordered peptide conformation.[27–35] Although less frequent, LPPs can also form nanotubes based on wrapping of β-sheet tapes.[26,36–42]

The present study builds on our prior research on LPPs bearing short bioactive lysine-rich peptide sequences. We studied the self-assembly and biological activity of a LPP bearing a lysine-rich collagen-stimulating pentapeptide KTTKS, used in Matrixyl™ formulations,[3,28,43] as well as the self-assembly

[a] *School of Chemistry, Food Biosciences and Pharmacy, University of Reading, Whiteknights, Reading, RG6 6AD, UK. E-mail: I.W.Hamley@reading.ac.uk*
[b] *School of Biological Sciences, University of Reading, Whiteknights, Reading, RG6 6AS, UK*
[c] *Nanomicroscopy Center, Aalto University, Puumiehenkuja 2, FIN-02150, Espoo, Finland*

† Electronic supplementary information (ESI) available: Additional cryo-TEM images and SAXS data, ThT fluorescence data, CD spectra, Tables of SAXS fit parameters and calculated pKa values. See DOI: https://doi.org/10.1039/d5sm00432b

of LPPs including shorter sequences such as C_{16}-KT and C_{16}-GHK.[44] We also investigated co-assembly with the LPP C_{16}-ETTES bearing oppositely charged glutamic acid residues replacing lysines.[45] The self-assembly of the related lipopeptides (peptide amphiphiles) C_{14}-KTTKS and C_{18}-KTTKS with distinct lipid chain lengths was also examined,[46] and most recently we have investigated the self-assembly and bioactivity and responsiveness to environmental triggers (UV radiation or chemical reductants) of lipoyl-KTTKS bearing a lipoic acid moiety at the N-terminus.[47] The K-rich LPP (containing a core fragment of the amyloid β peptide, KLVFF) C_{16}-KKFFVLK, self-assembles into nanotubes and helical ribbons which undergo a reversible unwinding transition upon increasing the temperature from 20 to 55 °C.[36] In a demonstration of enzyme-responsive nanostructural changes, this LPP can be cleaved by α-chymotrypsin at two sites leading to products C_{16}-KKF and C_{16}-KKFF, which do not self-assemble into nanotubes but instead form spherical micelles.[48] Later, C_{16}-KKFF was used to prepare alginate/graphene oxide capsules with selective antimicrobial activity towards the Gram-positive bacterium Listeria.[49] More recently, we modified KTTKS by attaching one or two cycloalkane chains (cycloheptadecyl or cyclododecyl) to the peptide sequence.[50] The cycloalkane-modified LPPs self-assemble to form globular structures or twisted nanotapes, depending on the number of cycloalkane chains, and the molecules show excellent compatibility with dermal fibroblasts with additional pro-vascularization capability.

We have recently studied the self-assembly, colloidal properties and antimicrobial activity of LPPs comprising a palmitoyl (hexadecyl, C_{16}) lipid chain attached to a lysine (K)-rich tripeptide.[11,12,35] Specifically, we compared the aggregation and properties of C_{16}-YKK, C_{16}-Ykk, C_{16}-WKK and C_{16}-Wkk. In these molecules, the cationic lysine (K) or D-lysine (k) residues promote self-assembly and are responsible for antimicrobial activity; whereas π-stacking interactions between tyrosine (Y) and tryptophan (W) residues promote aggregation and enable other interactions such as π–π or cation–π interactions. At acidic pH, all these LPPs self-assemble into micelles.[11,35] At basic pH, K-containing LPPs self-assemble into nanofibers, while k-containing lipopeptides self-assemble into nanotapes or nanotubes.[12] All four LPPs have antimicrobial activity against both Gram-negative and Gram-positive bacteria, with low values of the minimum inhibitory concentration (MIC) and favorable values of the selectivity index (haemolysis compared to the MIC), especially for the tryosine-containing lipopeptides.[11,12] The antimicrobial activities against Gram-positive and negative bacteria and fungi of lysine-rich LPPs including C_{16}-K, C_{16}-KKK and other tripeptide sequences and selected sequences containing k have been compared, and particularly potent activity (for all strains examined) was noted for C_{16}-KKK, although it also exhibits the highest haemolysis.[5] These authors also present a preliminary examination of nanostructures of selected lysine-rich LPPs (the tripeptide compounds) through transmission electron microscopy (TEM). The self-assembly of C_{16}-KK and C_{16}-KKK has been investigated by theoretical and experimental methods,[51] and these molecules can be used to prepare antimicrobial hydrogels.[52] The lipidated amino acid C_{16}-K (minimal lysine-based sequence, *i.e.* a single amino acid) shows a salt-dependent transition from self-assembled planar bilayers into scroll-like cochleates.[53] The antimicrobial and haemolysis activity of a series of lipidated conjugates of tripeptides KKK and KGK have been reported, with a range of lipid chains including C_{16} and other hydrocarbon and fluorocarbon chains.[54] A notable reduction in antimicrobial activity was observed in the presence of serum albumin, due to non-specific binding. The antimicrobial activities, lipid binding and micelle formation of C_{16}-KK, C_{16}-KGK and C_{16}-KKKK (all with an amidated C-terminus) have been compared by another group.[7] Later, other analogues with varied lipid chain lengths C_{12}–C_{18} and lysine-rich di- to tetra-peptide sequences were studied, and C_{16}-KKKK-NH_2 was found to have an optimal balance of hydrophobic and polar fragments leading to a good balance between antimicrobial and hemolytic activity.[55] Molecules bearing ''double headgroups'' of lysine residues (Y-shaped amphiphilic molecules with one or two lysines on each branch and a C_{16}-alkyl chain) have been introduced by the same group, and they also show good antimicrobial activity.[56] In another recent example, the self-assembly and antimicrobial and angiogenic activities of LPPs containing K-rich sequences from the amyloid β peptide have been demonstrated, along with the formation of injectable hydrogels.[9]

Here, we investigate the self assembly, cytocompatibility and antimicrobial activity of three LPPs, namely C_{16}-KFK, C_{16}-KWK and C_{16}-KYK (Scheme 1). This work builds on our previous study of related K-rich LPPs discussed in the paragraphs above. The secondary structure of the LPPs was studied using circular dichroism (CD) and fibre X-ray diffraction. Values of the critical aggregation concentration (CAC) were determined from surface tension experiments and fluorescence assays. The self-assembly motif was characterised using small-angle X-ray scattering (SAXS), cryogenic-transmission electron microscopy (cryo-TEM) and X-ray diffraction (XRD). Cell viability was studied through mitochondrial activity (MTT) assays and antimicrobial activity was assessed by determination of the minimum inhibitory concentration (MIC) and minimum bactericidal concentration (MBC) values.

Methods

Materials and sample preparation

Lipopeptides were purchased from BioservUK (Rotherham, UK) and supplied as TFA salts. The molar masses measured by ESI-MS are as follows: C_{16}-KFK 659.50 g mol^{-1} (660.60 g mol^{-1} expected), C_{16}-KWK 699.55 g mol^{-1} (698.51 g mol^{-1} expected) and C_{16}-KYK 676.50 g mol^{-1} (675.49 g mol^{-1} expected). The purity by HPLC (0.1% TFA in an acetonitrile/water gradient) is 97.2% for C_{16}-KFK, 96.5% for C_{16}-KWK and 95.5% for C_{16}-KYK. Solutions were prepared by dissolution in ultrapure water, leading to a pH of 2.3 for 1 wt% solutions of C_{16}-KWK and C_{16}-KYK and a pH of 2.5 for C_{16}-KFK. Samples at pH 8 were prepared by the addition of suitable amounts of 2M NaOH solution.

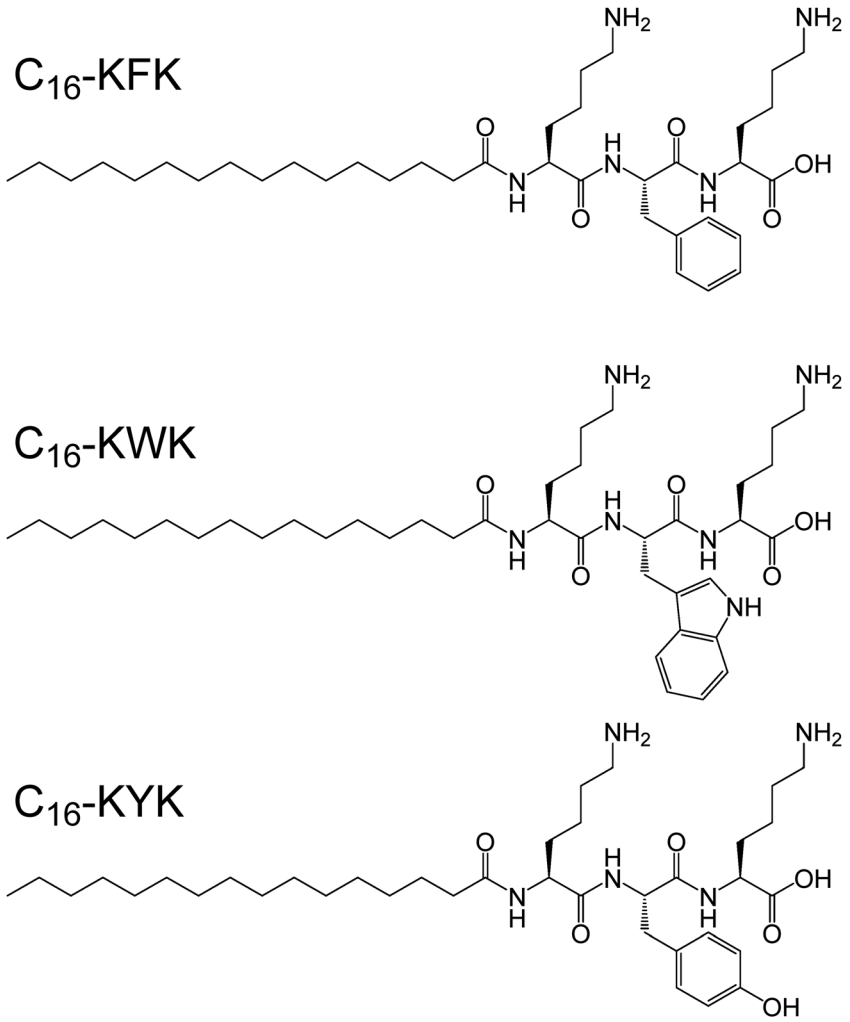

Scheme 1 Molecular structures.

Cryogenic-TEM (Cryo-TEM). Aliquots of 5 μL of the sample were applied to a freshly glow-discharged lacey carbon grid and plunge-frozen using a Leica GP2 plunge-freezer. The grids were imaged using a JEOL 2100Plus FS microscope (JEOL, Tokyo, Japan) with a Gatan OveView camera. Additional cryo-TEM was performed using a field emission cryo-electron microscope (JEOL JEM-3200FSC), operating at 200 kV. Images were taken in bright-field mode and using zero loss energy filtering (omega type) with a slit width of 20 eV. Micrographs were recorded using a Gatan Ultrascan 4000 CCD camera. The specimen temperature was maintained at −187 °C during the imaging. Vitrified specimens were prepared using an automated FEI Vitrobot device using Quantifoil 3.5/1 holey carbon copper grids with a hole size of 3.5 μm. Just prior to use, the grids were plasma cleaned using a Gatan Solarus 9500 plasma cleaner and then transferred into the environmental chamber of a FEI Vitrobot at room temperature and 100% humidity. Thereafter, 3 μL of the sample solution was applied on the grid and it was blotted twice for 5 seconds and then vitrified in a 1/1 mixture of liquid ethane and propane at a temperature of −180 °C. The grids with the vitrified sample solution were maintained at liquid nitrogen temperature and then cryo-transferred to the microscope.

Small-angle X-ray scattering (SAXS). SAXS experiments were performed on beamline B21[57] at Diamond (Didcot, UK). The sample solutions were loaded into the 96-well plate of an EMBL BioSAXS robot and then injected through an automated sample exchanger into a quartz capillary (1.8 mm internal diameter) in the X-ray beam. The quartz capillary was enclosed in a vacuum chamber, to avoid parasitic scattering. After the sample was injected into the capillary and reached the X-ray beam, the flow was stopped during the SAXS data acquisition. Beamline B21 operates with a fixed camera length (3.9 m) and fixed energy (12.4 keV). The images were captured using a PILATUS 2M detector. Data processing was performed using dedicated beamline software ScÅtter.

X-ray diffraction (XRD). Measurements were performed on stalks prepared by drying a drop of solution suspended between the ends of wax-coated capillaries. The stalks were mounted onto the four axis goniometer of an Oxford Diffraction Gemini Ultra instrument (Oxford Instruments, Abingdon, UK). The sample–detector distance was 50 mm and the X-ray wavelength

λ = 1.54 Å, used to calculate the scattering vector $q = 4\pi \sin\theta/\lambda$ (2θ: scattering angle). The detector was a Sapphire CCD.

Circular dichroism (CD) spectroscopy. Far-UV CD spectra were collected using a Chirascan spectropolarimeter (Applied Photophysics, Leatherhead, UK) equipped with a thermal controller. The spectra were recorded from 180 to 280 nm. Samples were mounted in a quartz cell with detachable windows, with a 0.01 or 0.1 nm path length and were also mounted in quartz cuvettes with a 1 mm path length. CD signals from the samples were corrected by water background subtraction. The CD spectra were smoothed using Chirascan Software for data analysis. The residue of the calculation was chosen to oscillate around the average, to avoid artifacts in the smoothed curve. CD data, measured in mdeg, were normalized to molar ellipticity using the molar concentration of the sample and the cell path length.

Fluorescence spectroscopy. To determine the values of the critical aggregation concentration (CAC), fluorescence assays were performed using Thioflavin T (ThT) since this dye binds to β-sheet fibrils and displays fluorescence.[58,59] Lipopeptides were prepared in 5×10^{-4} wt% ThT solution (λ_{ex} = 440 nm, measuring emission from 460 to 650 nm), and their fluorescence spectra were measured using a Varian Cary Eclipse Spectrofluorometer (Agilent, Didcot, UK).

Surface tension. The surface tension γ was measured by the Du Noüy ring method using a Krüss K12 processor tensiometer (Krüss, Hamburg, Germany). A dilution series was prepared from a concentrated stock solution. 3 ml of each solution were placed in a 25 ml beaker, and γ was manually measured for each concentration. The solution was left to equilibrate for 10 minutes before each measurement, before γ was measured from 3 ring detachments from the surface. The CAC was determined as the concentration at which γ reached a stable value. In addition, the slope below the CMC in the plot of γ against $\log_{10}(c)$ (c: concentration in [M]) was used to calculate the surface area per molecule at the air–water interface, A, according to the Langmuir adsorption equation for the surface excess:[60,61]

$$\Gamma = -\frac{1}{RT}\frac{\mathrm{d}\gamma}{\mathrm{d}[\log c]} \quad (1)$$

Here, R is the gas constant and T is the temperature. The surface area per molecule is obtained as

$$A = \frac{1}{\Gamma N_A} \quad (2)$$

where N_A is Avogadro's number.

Cell lines. L929 murine fibroblast cell lines (ECACC General Cell Collection) were grown in Dulbecco's modified Eagle's medium (DMEM) supplemented with 10% fetal bovine serum (FBS), 20 mM HEPES, and 1% GlutaMAX. The cells were maintained at pH 7.4, 37 °C, and 5% CO_2 in 25 cm^2 cell culture flasks.

Cytotoxicity assays. Cytotoxicity was investigated using an assay with 3-(4,5-dimethylthiazol-2-yl)-2,5-diphenyltetrazolium bromide (MTT) (Sigma-Aldrich, UK). Initially, L929 murine fibroblasts were maintained in Dulbecco's modified Eagle's medium (DMEM), supplemented with 10% fetal bovine serum (FBS), glutamine and penicillin–streptomycin, the reagents being purchased from Thermo Fisher Scientific (UK). The cells were seeded at a confluence of 5×10^3 cells in a volume of 100 μL per well into 96-well plates and incubated for 72 h in DMEM (10% FBS, 1% glutamine and 1% penicillin/streptomycin). After incubation, the cells were incubated for 4 h in DMEM without serum + 0.5 mg ml^{-1} MTT. The resulting formazan crystals were dissolved using 100 μL of DMSO for 30 minutes at 37 °C, protected from light. The resulting absorbances were read at 570 nm and the data were subsequently analyzed using GraphPad Prism software.

Antimicrobial activity. To determine the minimum inhibitory concentration (MIC) and minimum bactericidal concentration (MBC), a broth microdilution method was used to assess the antibacterial activity of the lipopeptides. Aliquots of 5 mL of overnight cultures of *E. coli* (ATCC 25922), *Salmonella enterica* (NCTC 5188), and *Staphylococcus aureus* (ATCC 12600) were prepared from isolated colonies previously grown on Luria–Bertani (LB) agar plates. Peptides were dissolved in sterile water and serially diluted in Mueller–Hinton (MH) broth to final concentrations ranging from 7.81 to 1000 μg mL^{-1}. Mid-log phase bacterial suspensions were adjusted to approximately 5×10^6 CFU mL^{-1} and added to 96-well plates containing solutions of each of the lipopeptides. Polymyxin B and water served as the positive and negative controls, respectively. The MIC was determined after 24 h of incubation at 37 °C by measuring the optical density at 600 nm using a Tecan Spark® microplate reader. To determine the MBC, aliquots from wells showing no visible growth were plated onto MH agar and incubated for an additional 24 h at 37 °C. All assays were performed in triplicate and repeated in at least three independent experiments.

Results and discussion

The self-assembled nanostructures of the LPPs were examined using cryo-TEM. Representative images for solutions at native pH (pH ≈ 2) and pH 8 are shown in Fig. 1 and additional images are shown in Fig. S1 (ESI†). The images show that C_{16}-KFK predominantly forms nanotube structures, although nested nanotube/cochleate structures as well as a small population of helical ribbon and twisted tape structures are observed in other regions of the grids. In contrast, C_{16}-KWK forms a dense array of twisted tape structures, whereas C_{16}-KYK shows a much less dense population of short (finite length) twisted tapes, resembling in some regions farfalle (bow-tie pasta)-like shapes. These morphologies are schematically illustrated in Fig. 2, along with the electron density across the bilayer used in the fitting of small-angle X-ray scattering (SAXS) data.

SAXS was used to provide an *in situ* complement to cryo-TEM, to probe the self-assembled nanostructure shapes and dimensions. The data for native pH (pH ≈ 2) are shown in Fig. 3a, along with form factor fits based on the lipopeptide

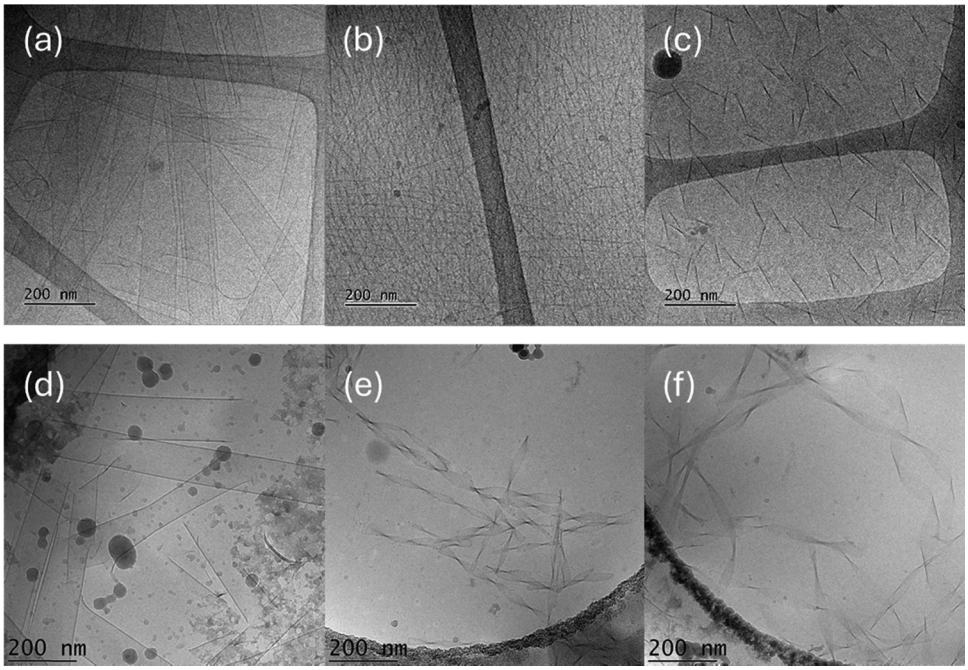

Fig. 1 Cryo-TEM images for 1 wt% samples at native pH (pH 2): (a) C_{16}-KFK, (b) C_{16}-KWK, (c) C_{16}-KYK, and at pH 8: (d) C_{16}-KFK, (e) C_{16}-KWK, (f) C_{16}-KYK.

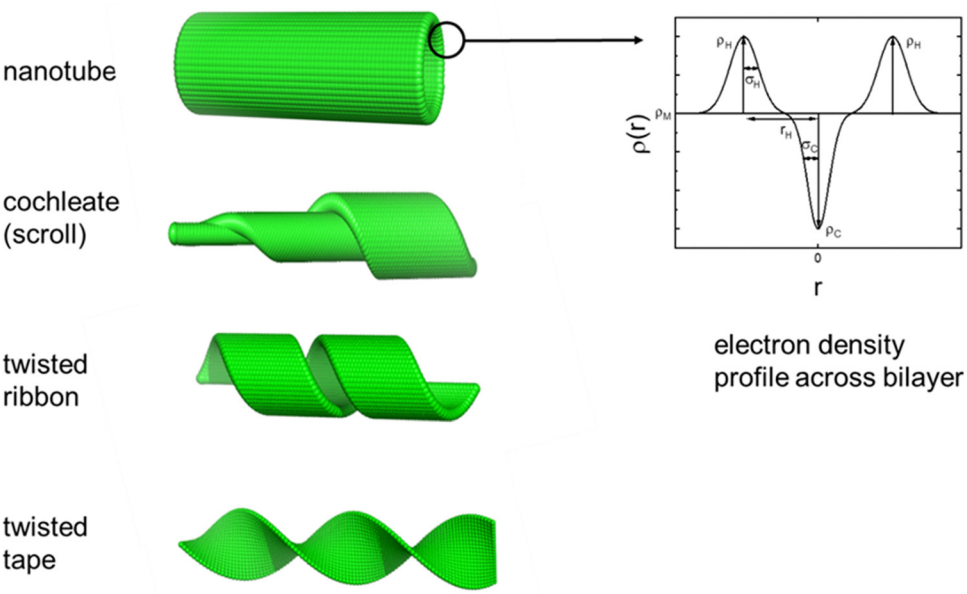

Fig. 2 Schematic of lipopeptide bilayer-based morphologies, and (right-hand side) schematic of three Gaussian functions to represent the bilayer electron density profile used in SAXS form factor modelling.

bilayer structures in nanotapes (for C_{16}-KWK and C_{16}-KYK) or nanotubes/cochleates (for C_{16}-KFK); these morphologies being those imaged by cryo-TEM. The data for all samples show an intensity scaling at a low wavenumber q, $I \sim q^{-2}$, consistent with the formation of planar bilayer structures.[62,63] In the previous work,[26,64,65] we have fitted SAXS data for LPP nanotube-forming systems to a form factor comprising that for a cylindrical shell and a Gaussian bilayer to allow for the variation in the LPP electron density across the bilayer. The latter is a combination of three Gaussian functions, representing the electron-poor lipid core of the bilayer and the electron-rich headgroup regions (Fig. 2). The sum of the hollow cylinder and Gaussian bilayer form factors represents an approximate convolution of the two terms and also allows for the presence of unclosed or partially closed nanotubes in many peptide and lipopeptide-based systems, for which twisted tape bilayers,

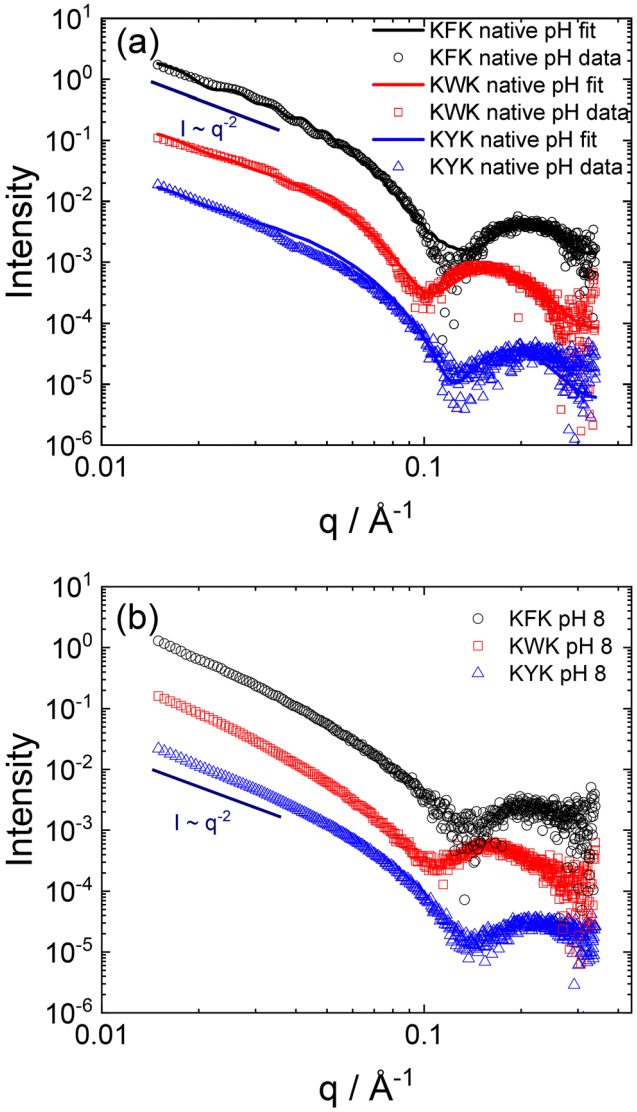

Fig. 3 SAXS data measured for 1 wt% samples (a) native pH (open symbols) along with fitted form factor (lines) as described in the text. (b) Measured data at pH 8. For convenience, only every 5th data point is shown and the data for C_{16}-KWK has been scaled by a factor 0.1, and that for C_{16}-KYK by a factor of 0.01.

scrolls ('cochleates'[53]) and ribbon structures are observed.[36,53,66,67] This model can be seen to fit the data satisfactorily, including the amplitude and position of the oscillations over much of the q range (except the peak at the lowest q, which may be influenced by structure factor), which arise due to the interference from the nanotube wall diameter and the form factor maximum at high q, which is due to the wall thickness. Consistent with the cryo-TEM results, which show twisted tape structures, the SAXS data for C_{16}-KYK and C_{16}-KWK can be fitted just using a Gaussian bilayer form factor to represent the structure within the nanotapes. The SAXS data at pH 8, shown in Fig. 3b, are very similar to those at native pH (and in fact nearly superpose and have the same low q scaling behaviour of a bilayer structure), consistent with the cryo-TEM images (Fig. 1), which show that the morphologies are stable across this pH range. Additional SAXS data were obtained at other pH values up to pH 12 and the data (Fig. S2, ESI†) show that the nanotape structure is retained across the range from the native pH to the highest pH measured (pH 10 or pH 12). Although there are, in some cases, changes in the sharpness of form factor maxima, and in some cases nanotube form factor maxima at low q; the intensity scaling at low q is $I \sim q^{-2}$.

To further probe the ordering within the remarkable nanotube structures formed by C_{16}-KFK, fibre XRD was performed. The pattern shown in Fig. 4 shows clear features resulting from the helical wrapping of the LPP in the nanotube walls, in particular the characteristic X-pattern of off-axis reflections from a helical structure (at $\pm 38^\circ$ with respect to the equator).[36,38,68,69] The equatorial reflections at 16.84 and 7.96 Å are assigned as the second and fourth orders of reflection from a lamellar structure with layer spacing 33 Å (the first order reflection can just be seen on the right-hand side of the 2D image), close to the layer spacing estimated from the fitting of the solution SAXS data (Table S1, ESI†). The presence of well-defined equatorial spacings along with a strong meridional reflection at d = 4.57 Å provides clear evidence for β-sheet structures,[36,45,70–72] while the other smaller d-spacings can also be assigned to spacings within β-sheet structures.[45,70,71]

The critical aggregation concentration (CAC) was next estimated using fluorescence probe measurements. Since cryo-TEM and SAXS indicate the formation of extended fibrillar types of nanostructures, we used Thioflavin T (ThT), a dye sensitive to the formation of 'amyloid' β-sheet structures.[59,73,74] The dependence of the peak fluorescence I (relative to the fluorescence of a reference ThT solution without lipopeptide, I_0) is plotted in Fig. 5 for the three LPPs (original fluorescence spectra are shown in Fig. S3, ESI†). The CAC for all three lipopeptides is the same within uncertainty, (0.01 ± 0.01) wt%. The data for C_{16}-KWK show lower intensities and more noise than the other two samples, which is ascribed to the possible mixing of fluorescence from the tryptophan residue and ThT. This may also affect the gradient of the fluorescence intensity *versus* concentration at low concentration values. Similar values for CAC for the LPPs are obtained at pH 8 (Fig. S4, ESI†).

The conformation and chirality of the tripeptides in the LPP assemblies (above the CAC) were investigated using circular dichroism (CD) spectroscopy. The spectra of 0.25 wt% samples at native pH (pH ≈ 2) are shown in Fig. 6, with additional spectra of samples at pH 8 in Fig. S5 (ESI†). The spectra at both pH values show similar features. The spectra of C_{16}-KFK and C_{16}-KYK show peaks in the range 210–240 nm, which are due to the n–π* and π–π* transitions in the aromatic Phe and Tyr groups;[75–78] however, such features are absent for C_{16}-KWK that shows a spectrum with a single broad negative maximum near 220 nm, which can be assigned in part to a red-shifted spectrum arising from β-sheet structures,[79] although there may also be a contribution from excitonic coupling. This sample forms a notably more dense network of fibrillar structures according to cryo-TEM and SAXS. The spectra of C_{16}-KWK and C_{16}-KYK show features similar to those reported for LPPs with the same residues in different sequences C_{16}-WKK and C_{16}-YKK reported

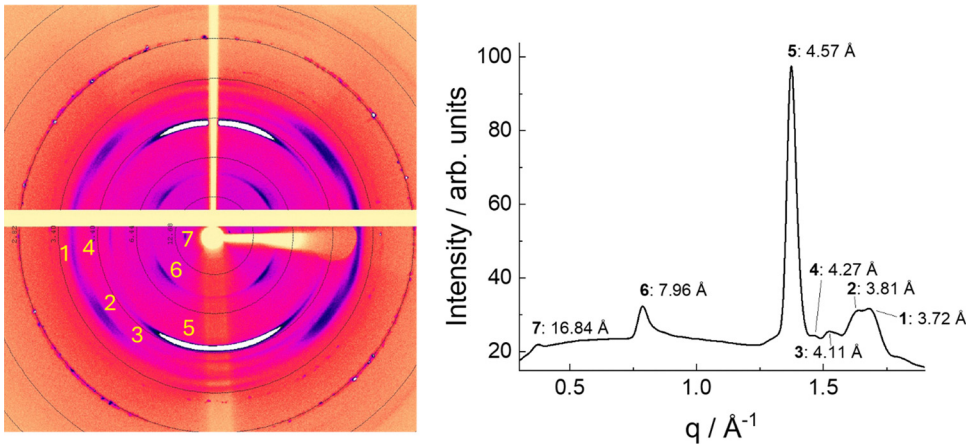

Fig. 4 Fiber XRD pattern from an aligned stalk prepared from a 1 wt% solution of C16-KFK (pH 4) along with one-dimensional intensity profile showing peak positions.

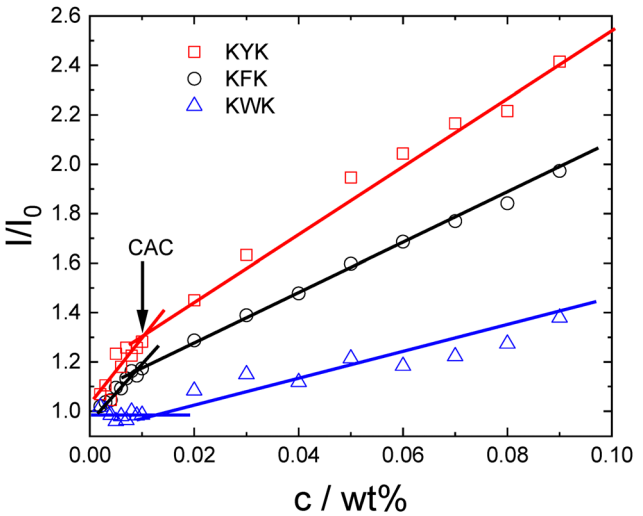

Fig. 5 ThT fluorescence peak intensity (I/I_0, where I_0 is the peak intensity for the ThT only solution) assay to determine critical aggregation concentration (CAC) of the three lipopeptides, as indicated, at native pH.

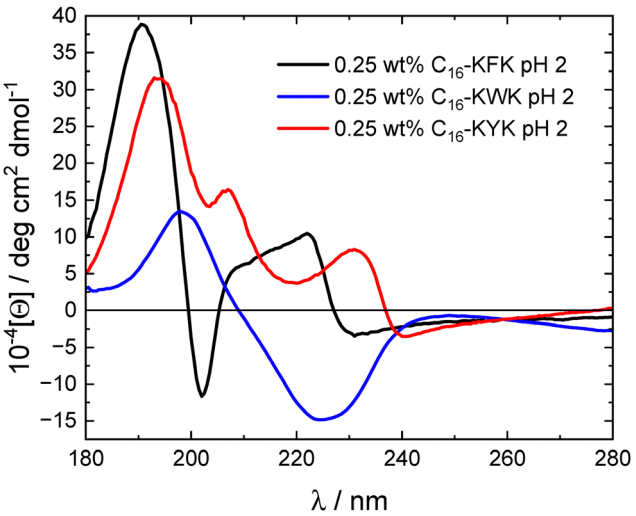

Fig. 6 CD spectra for 0.25 wt% samples, as indicated, at native pH.

previously.[12] The spectrum of C_{16}-KFK shows features previously analysed in detail for Fmoc-FF.[80] This includes some contribution from the excitonic coupling of L_α transitions, but it is heavily positively biased. The spectrum of C_{16}-KWK seems to have an excitonic couplet character with a slight negative bias, whereas this contribution for C_{16}-KYK is only positive. In summary, the CD spectra contain features of the excitonic coupling of the aromatic residues. For C_{16}-KFK and C_{16}-KYK, these features arising from the chiral environment of the Phe and Trp residues in the nanotube and twisted tape structures formed by these LPPs dominate, whereas C_{16}-KWK shows some features resembling those in classical β-sheet CD spectra.

To examine whether these cationic molecules act as biosurfactants, and to determine the CAC from an independent method, surface tension measurements were performed. The data shown in Fig. 7 show that all three LPPs behave as surfactants, reducing the surface tension from the value for pure water (72 mN m^{-1}), to less than 50 mN m^{-1}, with C_{16}-KWK showing the greatest activity, with a surface tension around 40 mN m^{-1} at the highest concentration studied. The CAC values indicated are in the range 0.01–0.02 wt% and are consistent with the values from the ThT fluorescence assays. The areas per molecule were also obtained from the Langmuir adsorption isotherm equation (eqn (1) and (2)) and are in the range 32.8–39.7 Å^2, which is reasonable for a lipopeptide packed in a monolayer at the air–water interface.[35]

The cytocompatibility of all three LPPs was determined using an MTT assay, a colorimetric assay based in the capacity of the eukaryotic cells to reduce tetrazolium salts into formazan crystals using mainly mitochondrial enzymes that can be used to evaluate the overall cell viability based on the mitochondrial metabolic activity.[81,82] Samples with concentrations from 0.0001 wt% to 0.05 wt% were evaluated and good cytocompatibility

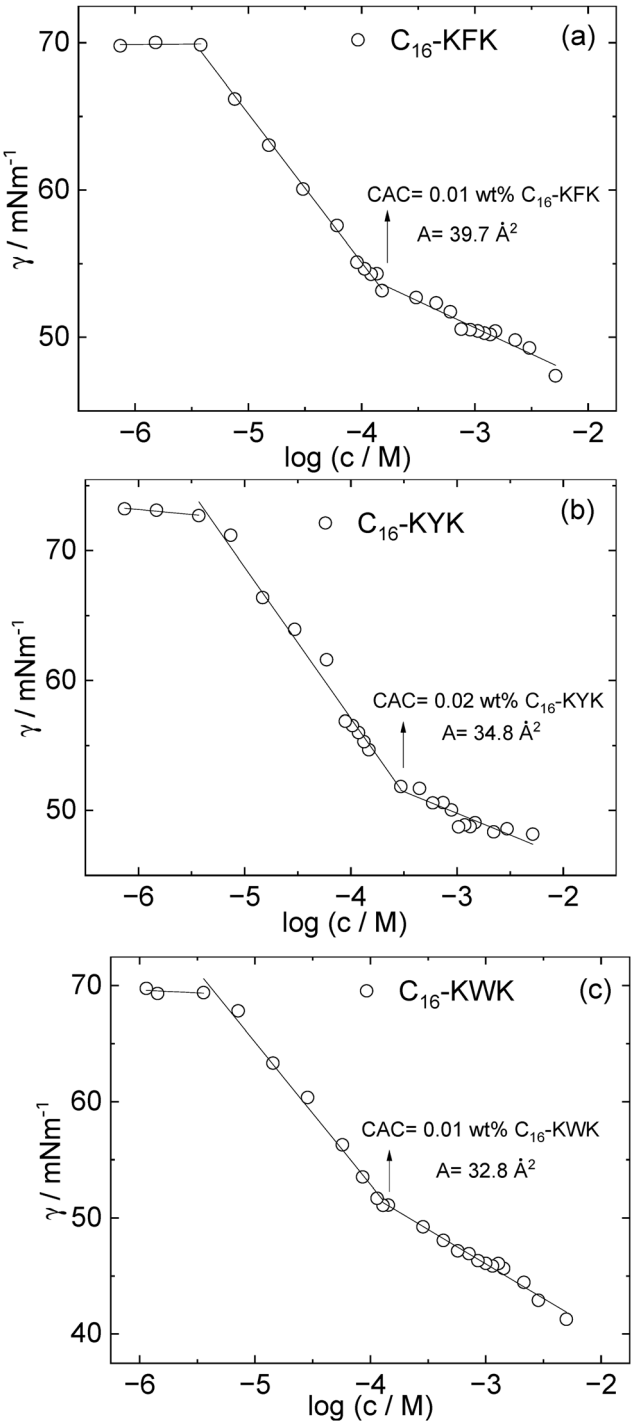

Fig. 7 Surface tension data (native pH). Langmuir adsorption isotherms for (a) C_{16}-KFK, (b) C_{16}-KYK and (c) C_{16}-KWK. Indicated are values of the CAC from the break points and the areas per molecule A from the slope of the lines below the CAC using the Langmuir adsorption isotherm equation (eqn (1) and (2)).

was found. As shown in Fig. 8, for most concentrations of any of the three LPPs, a non-significant decrease in cell viability is found, according to the Welch ANOVA. The only exceptions were cells incubated with C_{16}-KFK and C_{16}-KYK at 0.0125 wt% (Fig. 8a and b) and C_{16}-KWK at 0.0625 wt% (Fig. 8c).

The LPPs generally show good cytocompatibility to human cells (fibroblasts), which is one requirement to be useful as an antibiotic. We then investigated antimicrobial activity against Gram-positive and -negative species *via* determination of MIC and MBC values for the three LPPs. Contrary to the expectation for molecules bearing tripeptide sequences containing two cationic lysine residues, none of the molecules show substantial antibacterial activity against either Gram-positive *S. aureus* and *S. enterica* or Gram-negative *E. coli* (Table 1). This can be contrasted with our previous results[12] for C_{16}-YKK that shows an MIC of 31.25–62.5 μg ml^{-1} against the Gram-positive and Gram-negative strains studied (Table 1) or C_{16}-WKK that has a slightly higher MIC of 62.5 μg ml^{-1} except for *S. enterica* (Table 1). C_{16}-KFK, C_{16}-KWK and C_{16}-KYK were also tested against *P. aeruginosa* (PA01) and MRSA (methicillin-resistant *S. aureus*) and showed little activity, with MBC and MIC values $>$ 1000 μg ml^{-1} for all three LPPs.

Discussion and conclusions

In summary, C_{16}-KFK, C_{16}-KWK, and C_{16}-KYK form extended bilayer structures across a pH range from native acidic pH conditions to pH 8 and above. This can be contrasted with C_{16}-WKK and C_{16}-YKK (and analogues with D-lysine residues) that form micelles at native pH 4.6 but cylindrical fibrils at pH 8.[12] This points to the significant effects of the sequence in tuning the intermolecular interactions. To further examine whether the sequence influences the electrostatics, pK_a values were calculated using web software H++, which is based on continuum electrostatics or Poisson–Boltzmann calculations.[83,84] Insignificant differences in the predicted p*K*a values for the lysine ε-amino group (and tyrosine –OH and termini) are apparent on comparing C_{16}-KYK with C_{16}-YKK and C_{16}-KWK with C_{16}-WKK (Table S2, ESI†). Therefore electrostatic effects alone cannot explain the difference in self-assembly which is pH-sensitive for C_{16}-XKK but not C_{16}-KXK (X = W or Y and F in the latter case). The C_{16}-KXK LPPs form planar bilayer structures, whereas the C_{16}-XKK analogues form cylindrical fibrils at pH 8.[12] This is due to the differences in the packing and hydrogen bonding of the tripeptides for the two types of sequences.

The surface tension values for concentration values above the CAC, below 50 mM m^{-1} or 40 mM m^{-1} for C_{16}-KWK, are similar to those previously reported by us for C_{16}-WKK and C_{16}-YKK (and analogous lipopeptides with D-amino acid lysines).[35] However, it is important to note that here the lipopeptides self-assemble as nanotapes, whereas the previous studies on C_{16}-WKK and C_{16}-YKK were performed under conditions (native pH 4.6) where the lipopeptides form micelles. In fact, the determination of the CAC of fibrillar self-assembled peptide systems from surface tension measurements has been rarely reported (in one example, it has been demonstrated that amyloid β peptide fragments show surfactant properties[85]). The distinct one-dimensional fibrillization process may be responsible for the observation that the surface tension shows an inflection

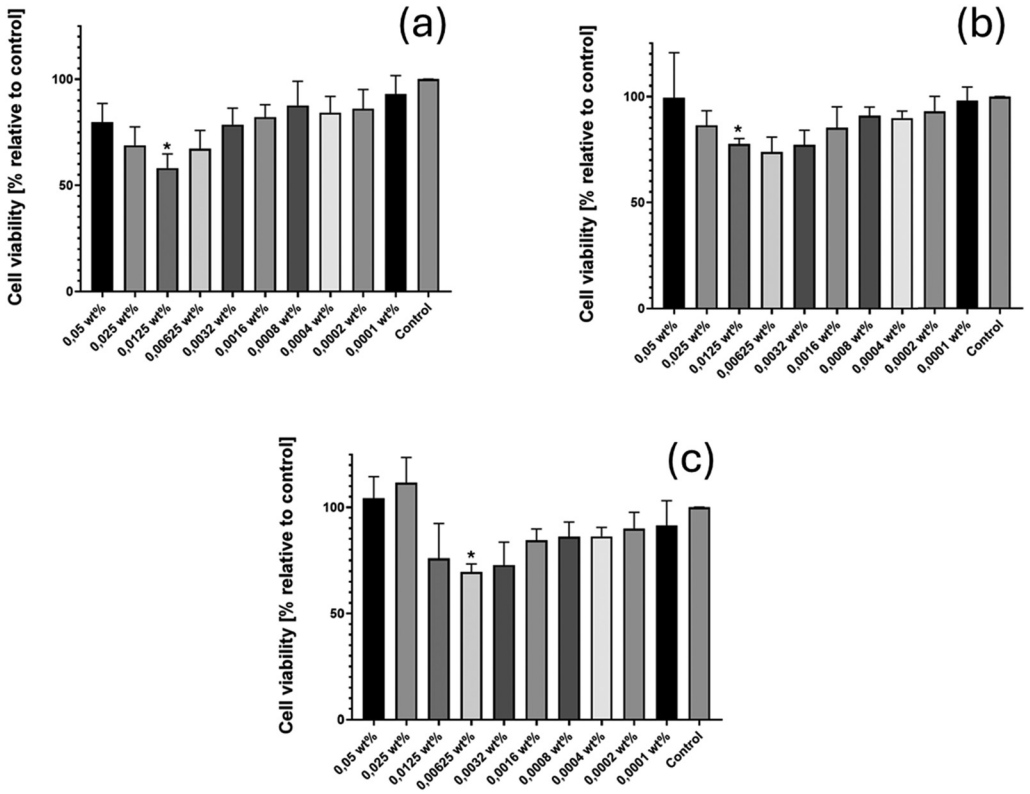

Fig. 8 MTT assays to determine the cytotoxicity of (a) C_{16}-KFK, (b) C_{16}-KYK and (c) C_{16}-KWK. The statistical analysis was performed by Welch ANOVA, n = 3 and Dunnet correction for multiple comparisons. * Indicates p equal or less than 0.05.

Table 1 Antimicrobial activity with comparison to previous data for C_{16}-YKK and C_{16}-WKK.[12]

	MIC ($\mu g\ mL^{-1}$)			MBC ($\mu g\ mL^{-1}$)		
Lipopeptide	*E. coli* (K12-ATCC 25922)	*S. enterica* (NCTC 5188)	*S. aureus* (ATCC 12600)	*E. coli* (K12-ATCC 25922)	*S. enterica* (NCTC 5188)	*S. aureus* (ATCC 12600)
C_{16}-KFK	>1000	>1000	>1000	>1000	>1000	>1000
C_{16}-KYK	500	>1000	500	1000	>1000	1000
C_{16}-YKK[12]	31.25-ND	62.5	62.5	62.5-ND	125	62.5
C_{16}-KWK	>1000	>1000	>1000	>1000	>1000	>1000
C_{16}-WKK[12]	62.5-ND	250	62.5	250	250	250

MIC = minimum inhibitory concentration is the lowest concentration that inhibits visible bacterial growth after incubation. MBC = minimal bactericidal concentration is the lowest concentration required to kill colony-forming units of bacterial population. ND = value not determined.

point (at the same concentration as the CAC from ThT dye fluorescence) rather than a point at which the surface tension levels off as in the case of a critical micelle concentration (CMC),[60,61] which corresponds to a closed association process into zero-dimensional spherical aggregates. The one-dimensional fibrillization is a nucleation and growth process with potential secondary nucleation and other events as described, for example, by the Oosawa model for homogeneous nucleation and one-dimensional growth.[86,87]

All three LPPs show good cytocompatibility to L929 fibroblasts; however, they showed unexpectedly low antimicrobial activity to either Gram-positive or Gram-negative species, as assessed *via* MIC and MBC determination. Clearly the sequence swap of two residues significantly influences the antimicrobial activity, as shown by the much lower activity for C_{16}-KXK compared to C_{16}-XKK (X = Y or W) reported in our previous paper[12] evident from the data in Table 1. With such cationic lipopeptides, this activity is believed to be mediated by interactions with oppositely charged membranes in the bacterial cell walls (Gram-positive bacteria lack an outer lipid membrane but have a peptidoglycan coating with a negative charge) and the sequences with two C-terminal lysines show much greater activity than those with the KXK pattern, where X is an aromatic residue. This is ascribed to the distinct modes of assembly of C_{16}-XKK and C_{16}-KXK at pH 8 (and across neutral pH relevant to the antimicrobial activity studies, see the SAXS data in Fig. S2, ESI†). Lipopeptides C_{16}-WKK and C_{16}-YKK form cylindrical fibrils, as evident from the SAXS data intensity scaling at a

low q, $I \sim q^{-1}$,[12] whereas C_{16}-KWK and C_{16}-KYK form bilayer nanotapes (SAXS intensity scaling $I \sim q^{-2}$). We propose that the difference in the curvature of the nanostructures influences the antimicrobial activity. Specifically, we suggest that the cylindrical fibrils (wormlike micelles or 'filomicelles'[88,89]) of C_{16}-XKK are able to induce a greater curvature in the bacterial membrane than the planar bilayer of C_{16}-KXK. The ability of cationic peptides to induce a curvature in lipid membranes is demonstrated,[90] and indeed proposed as one mechanism for the interaction of cationic cell-penetrating peptides with lipid membranes.[91,92] This is an interesting topic for future research on these systems, using model lipid membranes as in our previous work on surfactants—like arginine-based peptides.[4,93–95] The high-density presentation of peptide units at the surface of fibrils has been shown to promote delivery of active compounds and binding to targets *in vivo*, and thus there can be profound effects of the shape of self-assembled nanostructures on bioactivity, as discussed with examples, in a previous review.[96] Our results provide clear evidence that even subtle changes in sequences can profoundly influence both self-assembly (in particular, pH-dependence) and antimicrobial activity of designer lipopeptides with short cationic peptide motifs.

Conflicts of interest

The authors declare no competing interests.

Data availability

The data supporting this article have been included as part of the ESI.† Other data are available upon request from the authors.

Acknowledgements

This work was supported by the EPSRC Fellowship grant (reference EP/V053396/1) to IWH. We thank Diamond for the award of SAXS beamtime on B21 (ref. SM35585-1) and Nikul Khunti for assistance. We acknowledge the Warwick Advanced Bioimaging Research Technology Platform, for the use of the JEOL 2100Plus, supported by the MRC award reference MC_PC_17136, and Dr Saskia Bakker supported by EPSRC EP/V007688/1 for the images. We acknowledge the use of facilities in the Chemical Analysis Facility (CAF) at the University of Reading and Nick Spencer for assistance with XRD.

References

1 I. W. Hamley, *Chem. Commun.*, 2015, **51**, 8574–8583.
2 V. Castelletto, C. J. C. Edwards-Gayle, F. Greco, I. W. Hamley, J. Seitsonen and J. Ruokolainen, *ACS Appl. Mater. Interfaces*, 2019, **11**, 33573–33580.
3 R. R. Jones, V. Castelletto, C. J. Connon and I. W. Hamley, *Mol. Pharmaceutics*, 2013, **10**, 1063–1069.
4 V. Castelletto, R. H. Barnes, K. A. Karatzas, C. J. C. Edwards-Gayle, F. Greco, I. W. Hamley, R. Rambo, J. Seitsonen and J. Ruokolainen, *Biomacromolecules*, 2018, **19**, 2782–7294.
5 A. Makovitzki, J. Baram and Y. Shai, *Biochemistry*, 2008, **47**, 10630–10636.
6 G. Laverty, M. McLaughlin, C. Shaw, S. P. Gorman and B. F. Gilmore, *Chem. Biol. Drug Des.*, 2010, **75**, 563–569.
7 E. Sikorska, M. Dawgul, K. Greber, E. Ilowska, A. Pogorzelska and W. Kamysz, *Biochim. Biophys. Acta, Biomembr.*, 2014, **1838**, 2625–2634.
8 E. Kamysz, E. Sikorska, M. Jaskiewicz, M. Bauer, D. Neubauer, S. Bartoszewska, W. Baranska-Rybak and W. Kamysz, *Int. J. Mol. Sci.*, 2020, **21**, 887.
9 N. Mukherjee, S. Ghosh, J. Sarkar, R. Roy, D. Nandi and S. Ghosh, *ACS Appl. Mater. Interfaces*, 2023, **15**, 33457–33479.
10 C. Vicente-Garcia and I. Colomer, *Nat. Rev. Chem.*, 2023, **7**, 710–731.
11 A. Adak, I. W. Hamley, V. Castelletto, A. S. L. de Sousa, K.-A. Karatsas and C. Wilkinson, *Biomacromolecules*, 2024, **25**, 1205–1213.
12 A. Adak, V. Castelletto, B. Mendes, G. Barrett, J. Seitsonen and I. W. Hamley, *ACS Appl. Bio. Mater.*, 2024, **7**, 5553–5565.
13 H. G. Cui, M. J. Webber and S. I. Stupp, *Biopolymers*, 2010, **94**, 1–18.
14 J. B. Matson, R. H. Zha and S. I. Stupp, *Curr. Opin. Solid State Mater. Sci.*, 2011, **15**, 225–235.
15 J. B. Matson and S. I. Stupp, *Chem. Commun.*, 2012, **48**, 26–33.
16 M. J. Webber, E. J. Berns and S. I. Stupp, *Isr. J. Chem.*, 2013, **53**, 530–554.
17 E. Arslan, I. C. Garip, G. Gulseren, A. B. Tekinay and M. O. Guler, *Adv. Healthcare Mater.*, 2014, **3**, 1357–1376.
18 D. W. P. M. Löwik and J. C. M. van Hest, *Chem. Soc. Rev.*, 2004, **33**, 234–245.
19 F. Versluis, H. R. Marsden and A. Kros, *Chem. Soc. Rev.*, 2010, **39**, 3434–3444.
20 I. W. Hamley, *Soft Matter*, 2011, **7**, 4122–4138.
21 A. Trent, R. Marullo, B. Lin, M. Black and M. Tirrell, *Soft Matter*, 2011, **7**, 9572–9582.
22 M. P. Hendricks, K. Sato, L. C. Palmer and S. I. Stupp, *Acc. Chem. Res.*, 2017, **50**, 2440–2448.
23 J. D. Hartgerink, E. Beniash and S. I. Stupp, *Science*, 2001, **294**, 1684–1688.
24 E. T. Pashuck, H. Cui and S. I. Stupp, *J. Am. Chem. Soc.*, 2010, **132**, 6041–6046.
25 A. D. Ozkan, A. B. Tekinay, M. O. Guler and E. D. Tekin, *RSC Adv.*, 2016, **6**, 104201–104214.
26 E. Rosa, L. de Mello, V. Castelletto, M. L. Dallas, A. Accardo, J. Seitsonen and I. W. Hamley, *Biomacromolecules*, 2023, **24**, 213–224.
27 X. D. Xu, Y. Jin, Y. Liu, X. Z. Zhang and R. X. Zhuo, *Colloids Surf., B*, 2010, **81**, 329–335.
28 J. F. Miravet, B. Escuder, M. D. Segarra-Maset, M. Tena-Solsona, I. W. Hamley, A. Dehsorkhi and V. Castelletto, *Soft Matter*, 2013, **9**, 3558–3564.

29 I. W. Hamley, S. Kirkham, A. Dehsorkhi, V. Castelletto, M. Reza and J. Ruokolainen, *Chem. Commun.*, 2014, **50**, 15948–15951.
30 A. Dehsorkhi, V. Castelletto, I. W. Hamley, J. Adamcik and R. Mezzenga, *Soft Matter*, 2013, **9**, 6033–6036.
31 H. C. Fry, L. A. Solomon, B. T. Diroll, Y. Z. Liu, D. J. Gosztola and H. M. Cohn, *J. Am. Chem. Soc.*, 2020, **142**, 233–241.
32 I. S. Oliveira, M. Lo, M. J. Araújo and E. F. Marques, *Soft Matter*, 2019, **15**, 3700–3711.
33 J. A. Hutchinson, I. W. Hamley, J. Torras, C. Aleman, J. Seitsonen and J. Ruokolainen, *J. Phys. Chem. B*, 2019, **123**, 614–621.
34 J. N. B. D. Pelin, C. J. C. Edwards-Gayle, A. M. Aguilar, A. Kaur, I. W. Hamley and W. A. Alves, *Soft Matter*, 2020, **16**, 4615–4624.
35 I. W. Hamley, A. Adak and V. Castelletto, *Nat. Commun.*, 2024, **15**, 6785.
36 I. W. Hamley, A. Dehsorkhi, V. Castelletto, S. Furzeland, D. Atkins, J. Seitsonen and J. Ruokolainen, *Soft Matter*, 2013, **9**, 9290–9293.
37 I. W. Hamley, A. Dehsorkhi and V. Castelletto, *Chem. Commun.*, 2013, **49**, 1850–1852.
38 K. L. Morris, S. Zibaee, L. Chen, M. Goedert, P. Sikorski and L. C. Serpell, *Angew. Chem., Int. Ed.*, 2013, **52**, 2279–2283.
39 J. Madine, V. Castelletto, I. W. Hamley and D. A. Middleton, *Angew. Chem., Int. Ed.*, 2013, **52**, 10537–10540.
40 M. H. Koc, G. C. Ciftci, S. Baday, V. Castelletto, I. W. Hamley and M. O. Guler, *Langmuir*, 2017, **33**, 7947–7956.
41 A. Reja, S. P. Afrose and D. Das, *Angew. Chem., Int. Ed.*, 2020, **59**, 4329–4334.
42 I. W. Hamley, *Angew. Chem., Int. Ed.*, 2014, **53**, 6866–6881.
43 V. Castelletto, I. W. Hamley, J. Perez, L. Abezgauz and D. Danino, *Chem. Commun.*, 2010, **46**, 9185–9187.
44 V. Castelletto, I. W. Hamley, C. Whitehouse, P. Matts, R. Osborne and E. S. Baker, *Langmuir*, 2013, **29**, 9149–9155.
45 I. W. Hamley, A. Dehsorkhi and V. Castelletto, *Langmuir*, 2013, **29**, 5050–5059.
46 P. Palladino, V. Castelletto, A. Dehsorkhi, D. Stetsenko and I. W. Hamley, *Langmuir*, 2012, **28**, 12209–12215.
47 L. R. de Mello, V. Castelletto, L. Cavalcanti, J. Seitsonen and I. W. Hamley, *J. Pept. Sci.*, 2025, **31**, e70002.
48 A. Dehsorkhi, I. W. Hamley, J. Seitsonen and J. Ruokolainen, *Langmuir*, 2013, **29**, 6665–6672.
49 V. Castelletto, A. Kaur, I. W. Hamley, R. H. Barnes, K. A. Karatzas, D. Hermida-Merino, S. Swioklo, C. J. Connon, J. Stasiak, M. Reza and J. Ruokolainen, *RSC Adv.*, 2017, **7**, 8366–8375.
50 A. Adak, V. Castelletto, I. W. Hamley, J. Seitsonen, A. Jana, S. Ghosh, N. Mukherjee and S. Ghosh, *ACS Appl. Mater. Interfaces*, 2024, **16**, 58417–58426.
51 G. Zaldivar, S. Vernulapalli, V. Udumula, M. Conda-Sheridan and M. Tagliazucchi, *J. Phys. Chem. C*, 2019, **123**, 17606–17615.
52 G. Zaldivar, J. C. Feng, L. Lizarraga, Y. F. Yu, L. de Campos, K. M. P. de Oliveira, K. H. Piepenbrink, M. Conda-Sheridan and M. Tagliazucchi, *Adv. Mater. Interfaces*, 2023, **10**, 2300046.
53 C. R. Gao, S. Kewalramani, D. M. Valencia, H. H. Li, J. M. McCourt, M. O. de la Cruz and M. J. Bedzyk, *Proc. Natl. Acad. Sci. U. S. A.*, 2019, **116**, 22030–22036.
54 B. Findlay, G. G. Zhanel and F. Schweizer, *Int. J. Antimicrob. Agents*, 2012, **40**, 36–42.
55 O. Stachurski, D. Neubauer, A. Walewska, E. Ilowska, M. Bauer, S. Bartoszewska, K. Sikora, A. Hac, D. Wyrzykowski, A. Prahl, W. Kamysz and E. Sikorska, *Antibiotics*, 2022, **11**, 1491.
56 I. Maluch, O. Stachurski, P. Kosikowska-Adamus, M. Makowska, M. Bauer, D. Wyrzykowski, A. Hac, W. Kamysz, M. Deptula, M. Pikula and E. Sikorska, *Int. J. Mol. Sci.*, 2020, **21**, 8944.
57 N. P. Cowieson, C. J. C. Edwards-Gayle, K. Inoue, N. S. Khunti, J. Doutch, E. Williams, S. Daniels, G. Preece, N. A. Krumpa, J. P. Sutter, M. D. Tully, N. J. Terrill and R. P. Rambo, *J. Synchrotron Radiat.*, 2020, **27**, 1438–1446.
58 I. W. Hamley, *Angew. Chem., Int. Ed.*, 2007, **46**, 8128–8147.
59 H. Levine III, *Protein Sci.*, 1993, **2**, 404–410.
60 D. F. Evans and H. Wennerström, *The colloidal domain. Where physics, chemistry, biology and technology meet*, Wiley, New York, 1999.
61 I. W. Hamley, *Introduction to Soft Matter, Revised Edition*, Wiley, Chichester, 2007.
62 I. W. Hamley, *Small-Angle Scattering: Theory, Instrumentation, Data and Applications*, Wiley, Chichester, 2021.
63 A. Adak, V. Castelletto, L. de Mello, B. Mendes, G. Barrett, J. Seitsonen and I. W. Hamley, *ACS Appl. Bio. Mater.*, 2025, **8**, 803–813.
64 V. Castelletto, R. J. Gouveia, C. J. Connon and I. W. Hamley, *Faraday Discuss.*, 2013, **166**, 381–397.
65 V. Castelletto and I. W. Hamley, in *Peptide Self-Assembly: Methods and Protocols*, ed. B. L. Nilsson and T. M. Doran, Humana Press Inc, Totowa, 2018, vol. 1777, pp. 3–21.
66 J. Adamcik, V. Castelletto, I. W. Hamley and R. Mezzenga, *Angew. Chem., Int. Ed.*, 2011, **50**, 5495–5498.
67 L. Ziserman, H. Y. Lee, S. R. Raghavan, A. Mor and D. Danino, *J. Am. Chem. Soc.*, 2011, **133**, 2511–2517.
68 K. Lu, J. Jacob, P. Thiyagarajan, V. P. Conticello and D. G. Lynn, *J. Am. Chem. Soc.*, 2003, **125**, 6391–6393.
69 A. K. Mehta, K. Lu, W. S. Childers, S. Liang, J. Dong, J. P. Snyder, S. V. Pingali, P. Thiyagarajan and D. G. Lynn, *J. Am. Chem. Soc.*, 2008, **130**, 9829–9835.
70 M. Sunde, L. C. Serpell, M. Bartlam, P. E. Fraser, M. B. Pepys and C. C. F. Blake, *J. Mol. Biol.*, 1997, **273**, 729–739.
71 L. C. Serpell, *Biochim. Biophys. Acta, Biomembr.*, 2000, **1502**, 16–30.
72 I. W. Hamley, *Angew. Chem., Int. Ed.*, 2007, **46**, 8128–8147.
73 H. Levine, in *Methods in Enzymology*, ed. R. Wetzel, Academic Press, San Diego, 1999, vol. 309, pp. 274–284.
74 A. K. Buell, C. M. Dobson, T. P. J. Knowles and M. E. Welland, *Biophys. J.*, 2010, **99**, 3492–3497.
75 A. Rodger and B. Nordén, *Circular dichroism and linear dichroism*, Oxford University Press, Oxford, 1997.
76 M. Gupta, A. Bagaria, A. Mishra, P. Mathur, A. Basu, S. Ramakumar and V. S. Chauhan, *Adv. Mater.*, 2007, **19**, 858–861.
77 M. J. Krysmann, V. Castelletto and I. W. Hamley, *Soft Matter*, 2007, **3**, 1401–1406.

78 N. Amdursky and M. M. Stevens, *Chem. Phys. Chem.*, 2015, **16**, 2768–2774.
79 I. W. Hamley, D. R. Nutt, G. D. Brown, J. F. Miravet, B. Escuder and F. Rodríguez-Llansola, *J. Phys. Chem. B*, 2010, **114**, 940–951.
80 E. Hughes, N. S. O'Neill and R. Schweitzer-Stenner, *J. Phys. Chem. B*, 2024, **129**, 260–272.
81 T. Bernas and J. Dobrucki, *Cytometry*, 2002, **47**, 236–242.
82 M. Ghasemi, T. Turnbull, S. Sebastian and I. Kempson, *Int. J. Mol. Sci.*, 2021, **22**, 12827.
83 J. C. Gordon, J. B. Myers, T. Folta, V. Shoja, L. S. Heath and A. Onufriev, *Nucleic Acids Res.*, 2005, **33**, W368–W371.
84 R. Anandakrishnan, B. Aguilar and A. V. Onufriev, *Nucleic Acids Res.*, 2012, **40**, W537–W541.
85 B. Soreghan, J. Kosmoski and C. G. Glabe, *J. Biol. Chem.*, 1994, **269**, 28551–28554.
86 F. Oosawa and M. Kasai, *J. Mol. Biol.*, 1962, **4**, 10–21.
87 F. Oosawa and S. Asakura, *Thermodynamics of the polymerization of protein*, Academic Press, New York, 1975.
88 Y. Geng, P. Dalhaimer, S. S. Cai, R. Tsai, M. Tewari, T. Minko and D. E. Discher, *Nat. Nanotechnol.*, 2007, **2**, 249–255.
89 S. S. Cai, K. Vijayan, D. Cheng, E. M. Lima and D. E. Discher, *Pharm. Res.*, 2007, **24**, 2099–2109.
90 A. Yaghmur, P. Laggner, S. G. Zhang and M. Rappolt, *PLoS One*, 2007, **2**, e479.
91 N. Schmidt, A. Mishra, G. H. Lai and G. C. L. Wong, *FEBS Lett.*, 2009, **584**, 1806–1813.
92 A. Mishra, G. H. Lai, N. W. Schmidt, V. Z. Sun, A. R. Rodriguez, R. Tong, L. Tang, J. J. Cheng, T. J. Deming, D. T. Kamei and G. C. L. Wong, *Proc. Natl. Acad. Sci. U. S. A.*, 2011, **108**, 16883–16888.
93 V. Castelletto, R. H. Barnes, K.-A. Karatsas, C. J. C. Edwards-Gayle, F. Greco, I. W. Hamley, J. Seitsonen and J. Ruokolainen, *Langmuir*, 2019, **35**, 1302–1311.
94 C. J. C. Edwards-Gayle, V. Castelletto, I. W. Hamley, G. Barrett, F. Greco, D. Hermida-Merino, R. Rambo, J. Seitsonen and J. Ruokolainen, *ACS Appl. Bio. Mater.*, 2019, **2**, 2208–2218.
95 C. J. C. Edwards-Gayle, G. Barrett, S. Roy, V. Castelletto, J. Seitsonen, J. Ruokolainen and I. W. Hamley, *ACS Appl. Bio Mater.*, 2020, **3**, 1165–1175.
96 I. W. Hamley and V. Castelletto, *Bioconjugate Chem.*, 2017, **28**, 731–739.